Estimation of Nocturnal Boundary Layer Height in the Central Amazon, Supported by Gas Concentration Profiles

Carla M.A Souza[1,2], Anne C.S. Mendonça[2], Hella Van Asperen[1], Flávio A. F. D'Oliveira[3], Santiago Botía [1], Luís G. N. Martins[4], Denisi H. Hall[5], Raoni A. Santana[6], Gilberto Fisch[7], Leonardo R. Oliveira[5], Jailson R. Mata[5], Ranyelli Figueiredo[2,5], Rachel Albrecht[8], Bruno T. T. Portela[5], Carlos A. Quesada[5], and Cléo Q. Dias-Júnior[2,5]

[1]Max Planck Institute for Biogeochemistry, Jena, Thuringia, Germany
[2]National Institute of Amazonian Research (INPA), Graduate Program in Climate and Environment (CLIAMB), Manaus, Amazonas, Brazil
[3]Federal University of the State of Pará , Graduate Program in Environmental Sciences (PPGCA), Belém, Pará, Brazil
[4]Federal University of Santa Maria, Santa Maria, Rio Grande do Sul, Brazil
[5]National Institute of Amazonian Research (INPA), Large-Scale Biosphere-Atmosphere Program in the Amazon (LBA), Manaus, Amazonas, Brazil
[6]Federal University of Western Pará (UFOPA), Santarém, Pará, Brazil
[7]University of Taubaté, Taubaté, São Paulo, Brazil
[8]University of São Paulo, São Paulo, Brazil

Correspondence: Carla M.A Souza (calves@bgc-jena.mpg.de) and Cléo Q. Dias-Júnior (cleo.quaresma@inpa.gov.br)

Abstract.

The height of the nocturnal boundary layer (h_n) is a fundamental parameter for weather and climate prediction. However, because turbulent processes weaken at night, estimating h_n remains challenging. In addition, our understanding of its variability is limited, especially due to the predominant use of indirect methods that do not always accurately reflect the physical definition of the boundary layer. In this study we used micrometeorological measurements collected at the Amazon Tall Tower Observatory, in central Amazon. These measurements enable the study of turbulent sensible heat flux (H) profiles from the canopy top up to 300 m above ground, from which h_n can be defined. Our analysis focused on the seasonal differences between dry and wet periods for a La Niña year and an El Niño year. Also, we explore how variations in h_n affect the vertical distribution of CO and CH_4 concentrations. The results revealed significant variations, such as: largest values of h_n were observed during the wet season of a year marked by the La Niña phenomenon (∼270 m +/- 40 m), while smallest values of h_n occurred in the dry season associated with El Niño (∼100 m +/- 27 m). It was also observed that h_n can act as a "barrier" to the entry or exit of air masses with high concentrations of CO and CH_4. This study provides important insights into the variability of h_n above the Amazon forest, with implications for improving parameterizations in atmospheric models.

Keywords. Amazon Forest, Nocturnal Boundary Layer, Turbulent Flux Profiles, Trace Gases

1 Introduction

The Atmospheric Boundary Layer (ABL) is the lower part of the atmosphere that is in direct contact with the thermal and mechanical forcings that act near the surface (Garratt, 1980; Keirsbulck et al., 2002). The height of the ABL (z_i) plays an important role in the exchange of heat, moisture, gases and particles between the surface and the free atmosphere (Driedonks, 1982; Levi et al., 2020). Several studies have been carried out with the objective of estimating the height of the ABL, including for remote regions such as the Amazon (Fisch et al., 2004; Guo et al., 2016; Carneiro and Fisch, 2020; Krishnamurthy et al., 2020; Dias-Júnior et al., 2022; Molero et al., 2022; Souza et al., 2023). However, the majority of the studies carried out so far have given special attention to the variability of z_i during daytime, thus up to now there is little information about the variability of z_i during nighttime (Carneiro and Fisch, 2020; Mendonça et al., 2025).

The daytime variability of z_i is well known. For example, in the southwestern Amazon, Fisch et al. (2004) estimated z_i from radiosonde data as the height of the main inversion layer, identified from the vertical profile of potential temperature. They showed that z_i values differ between pasture and forest areas, with a deeper boundary layer over pasture, up to $\sim$1650 m, compared to forest, $\sim$1100 m. This contrast is attributed to differences in surface energy partitioning, since pasture areas exhibit higher sensible heat fluxes and lower evapotranspiration compared to forests, leading to stronger thermal turbulence and enhanced boundary layer growth. Carneiro and Fisch (2020) used 2 years of data collected during the Green Ocean Amazon (GoAmazon 2014/5) project campaign, carried out in the central Amazon, and observed that the maximum height of the convective boundary layer (CBL) was approximately 1,200 m in the wet season and approximately 1,600 m in the dry season. In addition to diurnal and seasonal variability, large-scale events such as El Niño and La Niña also influence the evolution of the boundary layer in the Amazon (Carneiro and Fisch, 2020; Dias-Júnior et al., 2022; Souza et al., 2023). During El Niño, the anomalous warming of the equatorial Pacific intensifies the occurrence of drier conditions, favoring a deeper CBL (Dias-Júnior et al., 2022; Souza et al., 2023). In contrast, during La Niña, greater moisture convergence favors increased precipitation that tends to limit its growth (Souza et al., 2023). Dias-Júnior et al. (2022) used ceilometer data, also collected during the GoAmazon project, and reported that daytime z_i values are maximum during the dry season in El Niño years.

The height of the boundary layer also plays an important role in the dispersion of pollutants near the surface. Based on ten years of measurements at 1,500 stations in China, Su et al. (2018) observed that z_i and particulate matter concentrations exhibit a negative correlation, indicating that deeper layers favor the dispersion of pollutants. In a complementary way, Miao et al. (2015) showed that the interaction between z_i and local circulations strongly modulates air quality in the Beijing–Tianjin–Hebei region. They showed that in autumn and winter, when z_i is generally shallower, and often combined with mountain breezes, it favors the accumulation of pollutants in the region. Meanwhile, in spring and summer, with deeper z_i and combined with the sea breeze, they promote more efficient dispersion conditions throughout the day.

On the other hand, the relationship between z_i and pollutants has been shown to be bidirectional. For example, Wang et al. (2019) observed that severe air pollution episodes occurred under conditions of weak winds, high humidity, and strong temperature inversions. The accumulation of aerosols reduced the incoming solar radiation and the sensible heat flux, which led to a weakening of vertical mixing and a 44–56 % reduction in z_i compared to clean days. Kulmala et al. (2023) in a study focused on boreal and Arctic regions within the framework of the Pan-Eurasian Experiment (PEEX), highlighted that the z_i also controls the vertical mixing and accumulation of trace gases such as CO_2, CH_4, and reactive volatile compounds. They emphasized that variations in z_i modulate near-surface concentrations of these gases, influencing local chemical reactivity and the radiative balance. Conversely, trace gases and aerosols can feedback on boundary-layer development by altering radiative fluxes, air temperature, and stability conditions.

To date, only a few studies have investigated the nocturnal boundary-layer height (h_n) above the Amazon rainforest. Santos et al. (2007), using radiosonde data measured in the southwestern Amazon, showed that h_n values were around 250 m. Dias-Júnior et al. (2022) using data from different instruments, showed that h_n values in the Central Amazon were 200 m. Recently, Mendonça et al. (2025) used turbulent sensible heat flux (H) profiles measured at 11 levels along the 325 m Amazon Tall Tower Observatory (ATTO) tower and reported that these profiles offer an opportunity to obtain direct measurements of h_n. These estimates are based on the height at which H falls below 5% of its near-surface value, unlike other methodologies that provide indirect measurements, such as radiosondes, ceilometers, and temperature profiles. The authors also observed that h_n varies according to atmospheric stability and local topography, with mean h_n values around ~ 80 m under very stable conditions and ~ 170 m under near-neutral conditions. Although the study by Mendonça et al. (2025) has contributed to recent advances in estimates of h_n values, the seasonal and interannual variability of h_n in the Central Amazon remains poorly understood. Moreover, no studies so far have directly addressed how h_n variability influences the near-surface vertical concentration profiles of trace gases.

In view of these gaps, the main objective of this study is to investigate the seasonal and interannual variability of h_n in the ATTO region during 2022 and 2023. In addition, it seeks to explore how variations in h_n affect the dispersion of selected trace gases in the region. This study extends previous analyses at the ATTO site by investigating the hourly evolution of h_n and its influence on near-surface trace gas concentrations. We believe that this work provides an important contribution to advancing knowledge in fields such as micrometeorology, aerosol dynamics, and greenhouse gas studies, all of which require precise descriptions of the structure of the Nocturnal Boundary Layer (NBL) (Santana et al., 2018; Botía et al., 2020; Barbosa et al., 2022; Franco et al., 2024).

2 Data and Methods

2.1 Experimental Site and Data Acquisition

The data used in this work were measured in 2022 and 2023 at the ATTO experimental site, located in the central Amazon, about 150 km northeast of Manaus, in the Uatumã Sustainable Development Reserve (SDR) (Figure 1a). The site is characterized by dense tropical forest with a relatively uniform canopy, whose tree crowns generally reach a height of around 37 m (Andreae et al., 2015; Gomes Alves et al., 2023). A detailed description of the site is provided by Andreae et al. (2015).

We used fast-response data (10 Hz) collected by sonic anemometers installed on two towers (located at 2.148° S, 59.0068° W, and 2.1448° S, 59.0008° W) that are 670 m apart (Dias-Júnior et al., 2019). The 81 m tower (INSTANT Tower) and the 325 m tower (ATTO Tower) are on a plateau, located at approximately 130 m above sea level (Chamecki et al., 2020). The sensors

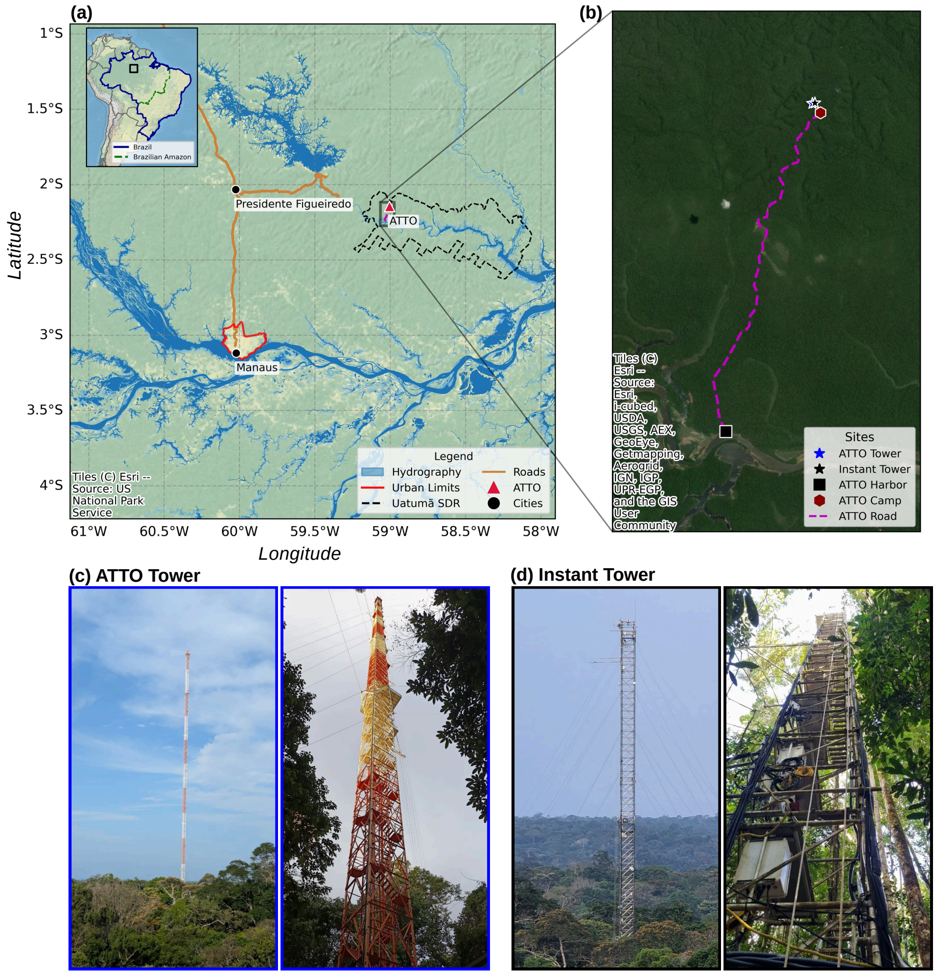

Figure 1. Geographic location and infrastructure of the Amazon Tall Tower Observatory (ATTO). a) Regional map showing the position of ATTO northeast of Manaus, within the Uatumã Sustainable Development Reserve (SDR); b) High-resolution zoom around the ATTO site based on Esri World Imagery, showing the ATTO Tower (blue star), Instant Tower (black star), ATTO harbor (black square), ATTO Camp (brown hexagon), and the ATTO access road (magenta dashed line); c) Photographs of the ATTO Tower (325 m) from ground perspective and structural details of its metallic frame; d) Photographs of the Instant Tower (80 m). All maps were generated using Python 3.11.6, in the WGS84 geographic coordinate system (EPSG:4326). Basemaps: Esri World Physical (panel a) and Esri World Imagery (panel b). Sources: Esri, TomTom, FAO, USGS | Powered by Esri.

used included CSAT-3B models from Campbell Scientific, Inc. (Logan, USA) installed at 50 and 81 m on the INSTANT Tower, and 3D Ultrasonic Anemometer model 4.3830 series from Thies Clima3D (Göttingen, Germany) installed at 100, 127, 151, 172, 223, 247, 274, and 298 m on the ATTO tower, all heights positioned above the ground. The variables measured were air temperature (T) and the three components of wind velocity (u, v, and w). Measurements from both towers were integrated into a single vertical profile, since previous studies did not identify significant differences between them (Mendonça et al., 2025).

Relative humidity and air temperature were obtained by thermohygrometers model IAKM I-Series from Galltec-Mela (Bondorf, Germany), and atmospheric pressure was recorded by barometers model 61302V (Young, USA), both operating at 0.01 Hz at the same heights as the anemometers. Net radiation (R_n) was calculated as the sum of the shortwave radiation components (incoming and reflected), measured by a CMP21 pyranometer, and the longwave radiation (incoming and emitted), recorded by a CGR4 pyrgeometer (both Kipp & Zonen, Delft, Netherlands). These measurements were carried out at 81 m on the INSTANT tower, at 0.01 Hz. CO and CH_4 concentrations were measured once per hour by a gas analyzer (FTIR Spectrometer) installed at the foot of ATTO tall tower, sampling air at five heights: 42, 81, 150, 273, and 321 m (van Asperen et al., 2023).Cloud fraction derived from the METEK MIRA-35C Cloud Radar Profiler and GOES-16 IR Channel 13 (10.3 μm) brightness temperature over the ATTO site were also used as complementary data for the case-study analysis. All analyses considered the nighttime period from 00 to 09 UTC (20 to 05 local time; UTC−4), avoiding transition intervals.

The main analyses were conducted for 2022–2023, when the complete sonic anemometer profile (up to 325 m) was available at ATTO. However, measurements of net radiation (R_n) at 81 m and turbulence measurements from the sonic anemometer at 50 m were available for the period 2016–2024 and were used to provide a broader climatological context.

2.2 Quality Control and Data Processing

As in other micrometeorological studies (Foken and Mauder, 2008; Starkenburg et al., 2016; Dias et al., 2023), the high-frequency data were initially segmented into 30-minute intervals (totaling 18 000 measurements) for the application of quality control (QC) procedures. QC was performed for each wind component and for the temperature measured by the sonic anemometers. The QC process included verification of record integrity, detection of error indicators, identification and removal of spikes, as well as the application of stationarity tests. For a detailed description of the quality control protocol adopted at the ATTO Site, it is recommended to consult Zahn et al. (2016) and Dias et al. (2023).

After QC, the planar fit method (Wilczak et al., 2001) was used for tilt correction. For each six-month period, wind velocity components were used to estimate the anemometer tilt angles and define a mean streamline coordinate system. The tilt-corrected wind vectors were then rotated for each 30-min interval to align the horizontal wind components with the mean wind direction (Kaimal and Finnigan, 1994). Subsequently, turbulence statistics were calculated over 5-min windows using Reynolds averaging, after applying linear detrending within each window. This shorter time window reduces the influence of non-turbulent motions, which are relevant under stable boundary-layer conditions (Sun et al., 2002; Oliveira et al., 2018).

H was obtained by the eddy covariance method (Webb et al., 1980), according to the equation: $H = \rho c_p \overline{w'T'}$, where ρ is air density (we assumed $1.225\,\mathrm{kg\,m^{-3}}$), c_p is the specific heat of air at constant pressure ($\mathrm{J\,kg^{-1}\,K^{-1}}$). The variables T' and w' represent the fluctuations of temperature and of the vertical wind component, respectively. The mean wind speed (U_m) was calculated as $U_m = \sqrt{u^2 + v^2}$, where u and v are the zonal and meridional wind components, respectively. The potential temperature (θ) was calculated as $\theta = T_h (p_0/P)^{R_d/c_p}$, where T_h is the air temperature measured by the thermohygrometer (Kelvin), P is atmospheric pressure (hPa), p_0 is the reference pressure (1000 hPa), and R_d is the gas constant ($287\,\mathrm{J\,kg^{-1}\,K^{-1}}$). Profiles of H were used to estimate h_n, while U_m and the vertical gradient of θ were used to discuss its variability.

Atmospheric stability was evaluated using the Monin–Obukhov stability parameter (z/L), where L represents the Obukhov length, determined as $L = -u_*^3 T/(kg\overline{w'T'})$, with u_* the friction velocity, k the von Kármán constant (0.41), g the acceleration due to gravity, and $\overline{w'T'}$ the kinematic sensible heat flux. The parameter z/L was calculated considering the variables u_*, $\overline{w'T'}$, and T at 50 m, similar to that performed by Cava et al. (2022). Vertical wind shear (dU/dz) was quantified from third-order polynomial fits applied to the wind speed profiles, from which analytical vertical derivatives were calculated.

2.3 Data Filtering and Classification

After QC and calculation of turbulence statistics, two filters were applied to the dataset of the 5 min. First, to avoid the influence of extreme values, outliers in the H measurements were identified by means of histograms by height layer. Based on the observed distribution, the filtering limits were defined empirically, resulting in the following specific ranges: from 50 to 81 m (-50 to $0\,\mathrm{W\,m^{-2}}$), from 100 to 151 m (-30 to $10\,\mathrm{W\,m^{-2}}$) and from 172 to 298 m (-20 to $10\,\mathrm{W\,m^{-2}}$). Values outside these ranges were considered outliers and removed from the analysis. To test the sensitivity of h_n to these filtering limits, we applied a more permissive scenario (-60 to 20, -45 to 25, and -35 to 15 W $\mathrm{m^{-2}}$; Scenario 2) and a more restrictive scenario (-30 to 0, -20 to 5, and -10 to 5 W $\mathrm{m^{-2}}$; Scenario 1) for the three height ranges. The normalized profiles were very similar, and the estimated h_n differed by less than 15 m among scenarios (Fig. S1), indicating that the results are robust to the selected thresholds. The application of differentiated limits reflects the expected variation of H among the layers, being more intense in the lower layers due to direct interaction with the canopy, and smoother at higher altitudes (Gao et al., 1989; Shaw and Schumann, 1992; Mendonça et al., 2025).

The second filter considered very stable atmospheric conditions, characterized by very low sensible heat fluxes above the canopy, indicative of minimal energy exchange, configuring a strongly decoupled regime (Cava et al., 2022). In these situations, the vertical profile of H does not present a typical structure (higher values near the canopy and a decrease with height), but rather an irregular pattern, which makes the reliable determination of h_n difficult. So, cases in which the H values at 50 m were between 0 and $-6\,\mathrm{W\,m^{-2}}$ were excluded, a range identified as the most frequent based on the data distribution under very stable conditions ($1 \leq z/L \leq 10$, such as Mendonça et al. (2025)).

Subsequently, the data were classified by seasonal period (Dry and Wet) in each year, with 2022 associated with La Niña and 2023 with El Niño (Table 1). According to the NOAA Climate Prediction Center, La Niña conditions persisted from late 2021 to early 2023, whereas a strong El Niño developed around May 2023 and lasted until early 2024. In the central Amazon, La Niña typically brings wetter conditions and slightly cooler temperatures, while El Niño tends to produce drier and warmer conditions, particularly during the Dry season, due to reduced convective activity and changes in large-scale atmospheric circulation (Marengo et al., 2018; Jimenez et al., 2018).

The Dry period was defined as the months of August, September, and October, and the Wet period encompassed the months of January to April. The inclusion of January is justified by the scarcity of data available in April, which could compromise the robustness of the analyses. Considering that January still falls within the region's Wet season, its inclusion increases the representativeness of the data. Moreover, Dias-Junior et al. (2026) showed that January remains among the rainiest months for ATTO's area. This division aligns with regional seasonal precipitation patterns in the Central Amazon described by Marengo

Table 1. Total number of 5-minute profiles and percentage of profiles excluded after data filtering.

Year	Period	Total number of profiles	Excluded profiles (%)
2022	Wet	6425	13
2022	Dry	7811	27
2023	Wet	7080	31
2023	Dry	6603	28

et al. (2001) and, for ATTO specifically, by Dias-Junior et al. (2026). From this classification, hourly means of all analyzed variables were calculated at their respective measurement heights.

2.4 Estimation of the Height of the Nocturnal Boundary Layer

After filtering and classification, hourly mean profiles of H were obtained from the 5-min data, allowing the estimation of h_n for each hour of the nighttime period, separately for the Dry and Wet seasons of 2022 and 2023. Since the sensible heat flux is greater near the canopy and decreases with height, h_n was identified as the height at which H was less than 5 % of the H value measured near the canopy (50 m) (Lenschow et al., 1988; Mendonça et al., 2025). This turbulence-based approach is consistent with the fundamental definition of the atmospheric boundary layer. To allow comparison among profiles, the H values at all heights were normalized by the value measured at 50 m ($H_{50\,\mathrm{m}}$).

In addition to the seasonal and hourly analyses, we selected two nights as case studies to investigate the relationship between variability in h_n and the vertical concentration profile of CO and CH_4: one with a shallow h_n layer ($h_n \sim 80$ m) and another with a deeper layer ($h_n \sim 150$ m). The idea here was to investigate to what extent h_n affects the temporal and spatial gas concentration variations along the tower.

3 Results

3.1 Atmospheric Stability at the ATTO Site

Figure 2 shows the hourly mean values of R_n and stability parameter (z/L) for the Wet and Dry periods in the years 2022 and 2023. Both the Wet and Dry seasons of 2022 presented R_n values with larger magnitude than those observed in the Wet and Dry seasons of 2023 (Fig. 2a, b). In addition, $|R_n|$ values for the Dry season are greater than those observed in the Wet season, in both years. Cloud cover has a direct relationship with R_n values (Barber and Thomas, 1998; Von Randow et al., 2004; De Oliveira et al., 2016). Greater cloud cover is associated with lower radiative loss, that is, smaller $|R_n|$ values. Therefore, in the Dry season, where cloud cover is lower, there is greater radiative loss. The same reasoning applies to the year 2023, an El Niño year characterized by reduced cloud cover over the central Amazon (Jimenez et al., 2018; Restrepo-Coupe et al., 2023). Atmospheric stability also varies systematically between seasons (Fig. 2c, d). The Wet period is less stable

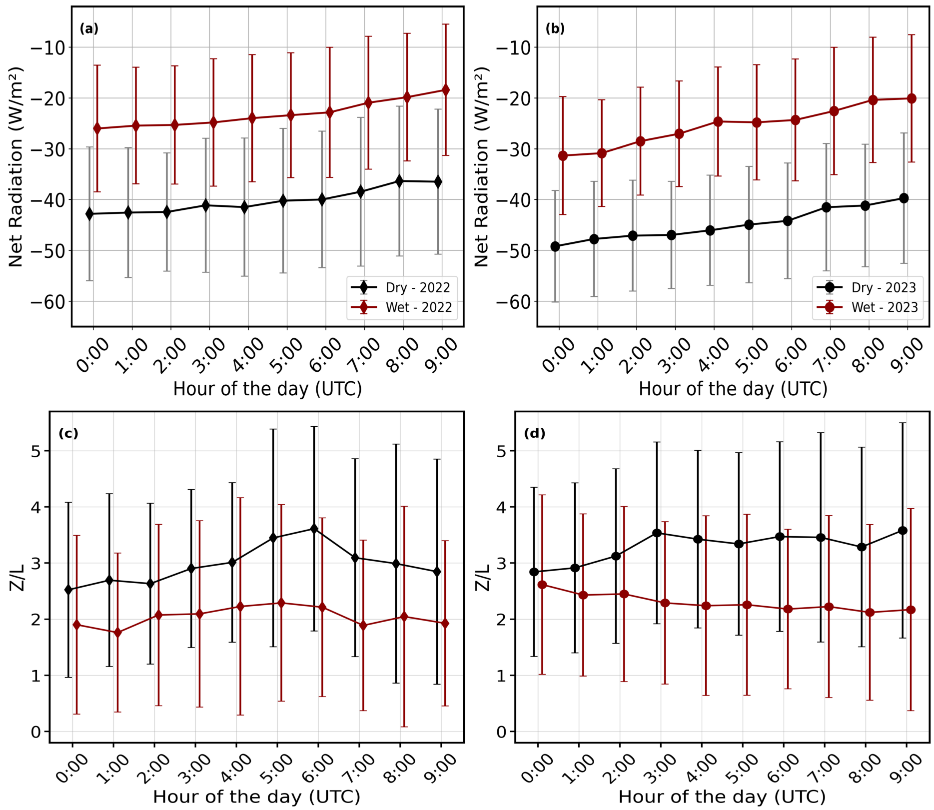

Figure 2. Hourly mean values of (a,b) net radiation (R_n) measured at 81 m and (c,d) stability parameter (z/L) calculated at 50 m for the Wet season (red) and the Dry season (black) during 2022 (left panels) and 2023 (right panels). The bars indicate the standard deviation.

(smaller $z/L = 2.15$), while the Dry period shows stronger stability ($z/L = 3.10$) consistent with enhanced radiative cooling and reduced turbulent mixing. El Niño in 2023 enhanced this effect (Fig. 2d).

To place the analyzed years in a broader climatological context, Figure 3 shows the monthly nocturnal climatology of R_n and z/L for the 2016–2024 period, using the same nighttime interval adopted in this study (00:00–09:00 UTC). The climatology highlights a clear seasonal cycle, with stronger nocturnal radiative cooling during the dry season associated with higher z/L values and therefore more stable atmospheric conditions. In 2023, z/L values were higher than the climatological mean during most months, especially from May onward, whereas 2022 remained closer to, or below, the climatological mean values. These departures from the ATTO climatology indicate that the two analyzed years experienced distinct nocturnal radiative cooling and stability conditions. Since R_n and z/L are relevant controls on turbulence intensity and the vertical structure of the nocturnal boundary layer, these differences may be related to the contrasting h_n behavior observed in 2022 and 2023 (discussed in section 3.2).

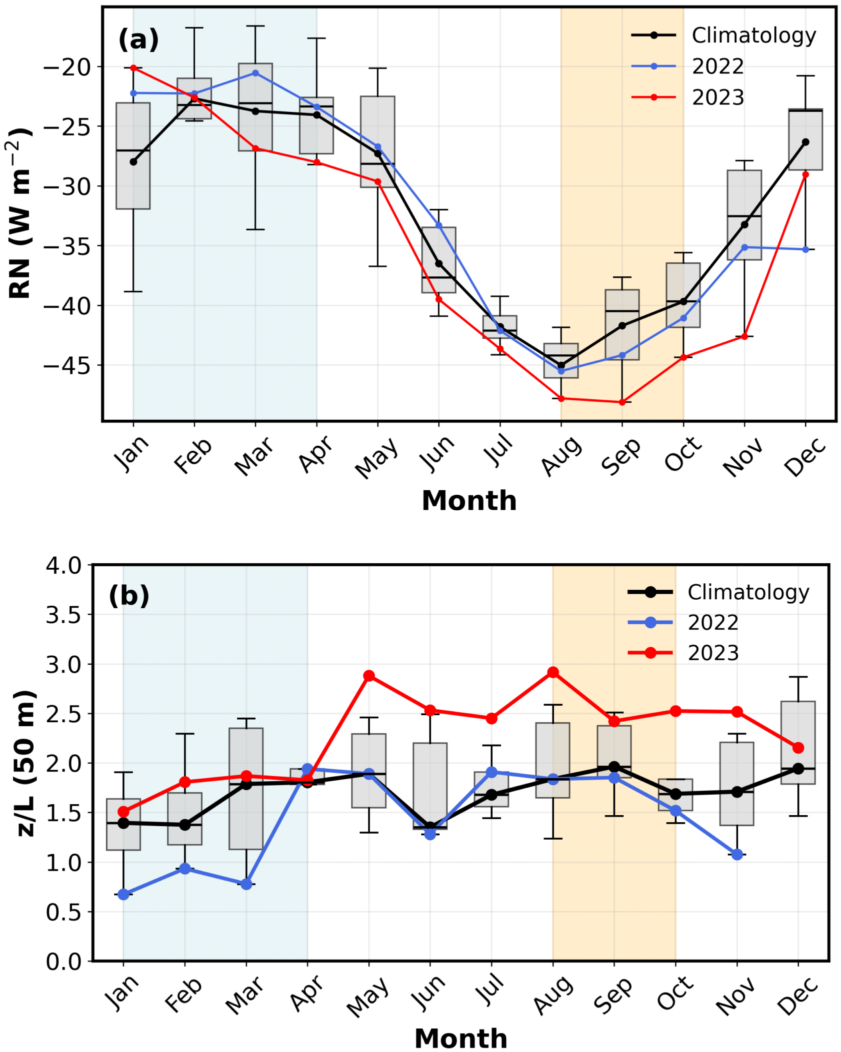

Figure 3. Monthly mean of (a) net radiation (R_n) at 81 m and (b) stability parameter (z/L) at 50 m for the nighttime period (00:00–09:00 UTC). Grey boxplots represent the monthly climatological distribution for 2016—2024. Shaded blue and orange areas indicate the wet and dry seasons, respectively.

3.2 Seasonal Mean Cycle of NBL Height

Figure 4 presents the normalized vertical profiles of sensible heat (H/H_{50}). The turbulent heat fluxes cease at different heights when comparing the Dry and Wet seasons, which indicates important seasonal variations of h_n. During the Wet period, turbulence extends up to approximately 200 ± 33 m in 2022 and 150 ± 24 m in 2023, while in the Dry period this height is reduced to about 120 ± 28 m in 2022 and 100 ± 21 m in 2023.

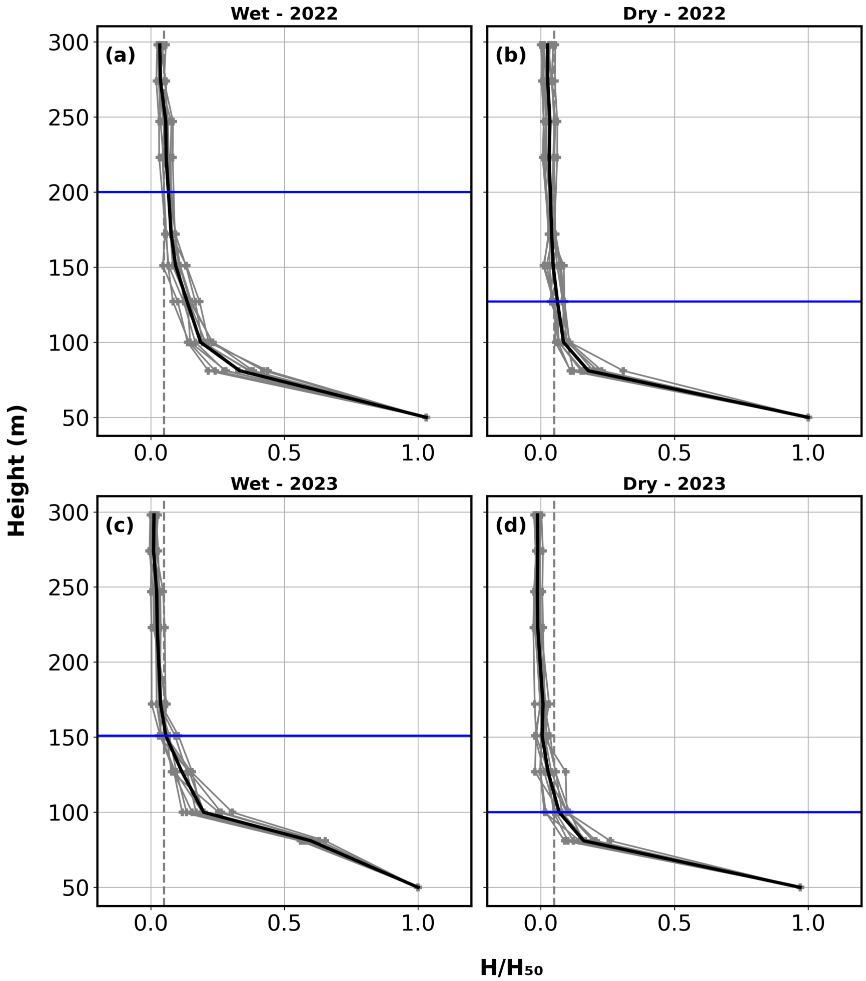

Figure 4. Hourly profiles of normalized sensible heat flux (H/H_{50}) for (a) Wet season 2022, (b) Dry season 2022, (c) Wet season 2023, and (d) Dry season 2023. Grey curves represent the individual hourly nighttime profiles, illustrating the variability in the vertical distribution of H/H_{50} throughout the night. The bold solid curve in each panel shows the seasonal mean profile. The vertical dashed grey line marks the 5 % threshold ($H/H_{50} = 0.05$), and the horizontal blue line marks the seasonal mean height at which this threshold is reached, interpreted as the h_n.

Figure 5 presents the hourly mean values of h_n for the Wet and Dry periods for the two years analyzed here. In 2022, h_n exhibited seasonal variations, being 274 m at the beginning and 151 m at the end of the night during the Wet season, while in the Dry season the values range between 223 m (beginning of the night) and 100 m (end of the night). In 2023, the seasonal variation of h_n is smaller between the seasons, ranging between 172 m at 00:00 UTC and 100 m at 09:00 UTC. In addition, regardless of the season or the year, the h_n values are higher at the beginning of the night and decrease progressively.

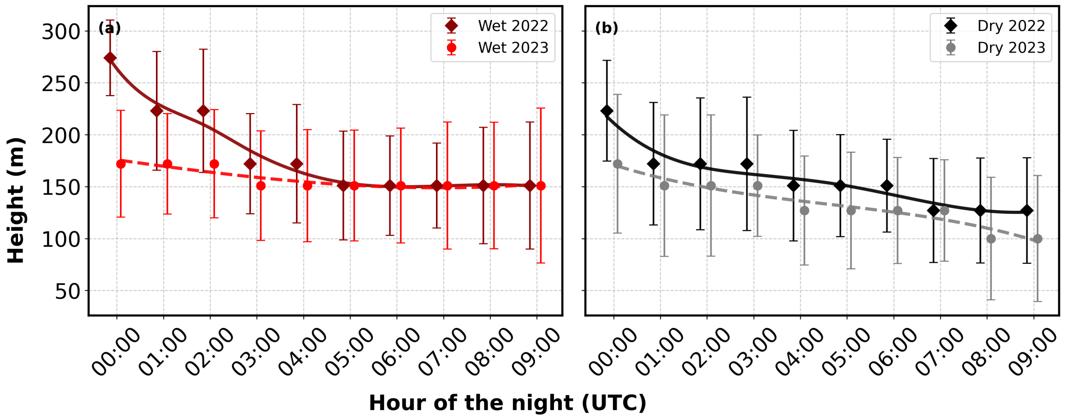

Figure 5. Mean values and standard deviation of h_n for (a) the Wet period of 2022 and 2023 and (b) the Dry period of 2022 and 2023. The curves represent smooth fits obtained by spline between the mean h_n values.

3.3 Temporal Variability of NBL Height and Its Relationship with Greenhouse Gas Concentrations Near the Surface: Case Studies

In general, h_n shows a gradual decrease throughout the night (Fig. 5). However, these changes in h_n values can be reflected in the vertical profiles of trace gasesmeasured along the tower.In order to explore this relationship, we refer to Figure 6, which shows two case studies: one in which the h_n values remained low throughout the entire night (18 August 2022), with values around 81 m, and another in which h_n showed a progressive increase from about 100 m to 170 m throughout the night (25 August 2022).

The wind profiles (Figure 7) show the occurrence of low-level jets (LLJs) on both nights, but with distinct characteristics. On the night of 18 August, the jet nose (maximum speed in the wind profile) was located at a height that oscillated around 80 to 100 m, while on the night of 25 August the jet nose was located around 170 m. Another important difference is observed in the dominant wind direction during the two nights (Figure 8). During the night of 18 August, the predominant wind direction was from the northeast at the lowest levels and from the southeast at the highest levels. During the night of 25 August, the wind direction ranged between north and northeast from the top of the canopy up to 298 m. According to Mendonça et al. (2026), the jet nose (maximum speed in the wind profile) can serve as an indicator of h_n, which is consistent with what we observe in our case studies.

To better identify the main drivers controlling the contrasting h_n behavior during the two case-study nights, we further analyzed R_n at 81 m, cloud cover, the vertical profile of θ and wind shear (dU/dz) (Fig. 9). These variables provide complementary information on the local radiative forcing, cloud modulation of nocturnal cooling, thermal stratification, and mechanical turbulence generation. The night of 18 August 2022 was characterized by strong nocturnal radiative cooling (Fig. 9a), reduced cloud occurrence (Fig. 9c and Fig. S2), and a pronounced vertical potential temperature gradient (Figure 9e). These conditions indicate enhanced thermal stratification near the surface. Although wind shear was observed at some levels (Fig. 9g), the strong

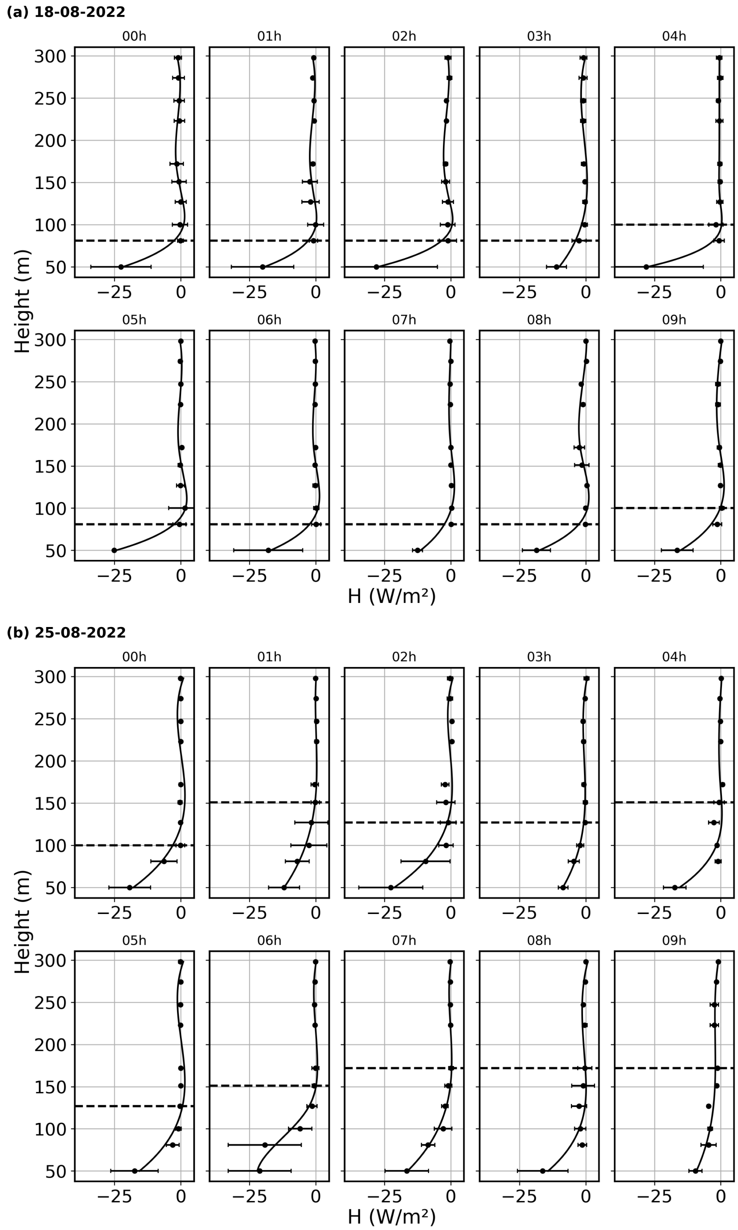

Figure 6. Hourly mean profiles of sensible heat flux (black curve), standard deviation, and the corresponding h_n (horizontal dotted lines) for a) 18 August 2022 and b) 25 August 2022.

stratification suggests that mechanically generated turbulence aloft was not efficiently coupled downward toward the canopy. This supports the interpretation that the shallow h_n observed on 18 August 2022 reflects not only strong thermal stratification, but also canopy-induced suppression of vertical mixing near the forest top. This configuration is consistent with a shallow

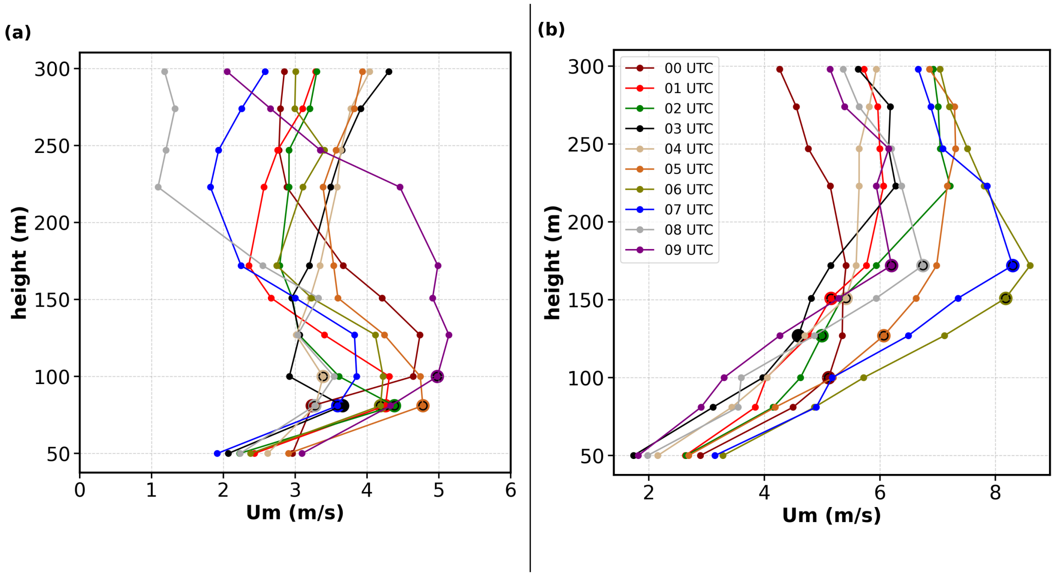

Figure 7. Hourly mean wind speed profiles for a) 18 August 2022 and b) 25 August 2022. The different colors indicate the different hours. The larger hollow circles mark the hourly estimates of the h_n.

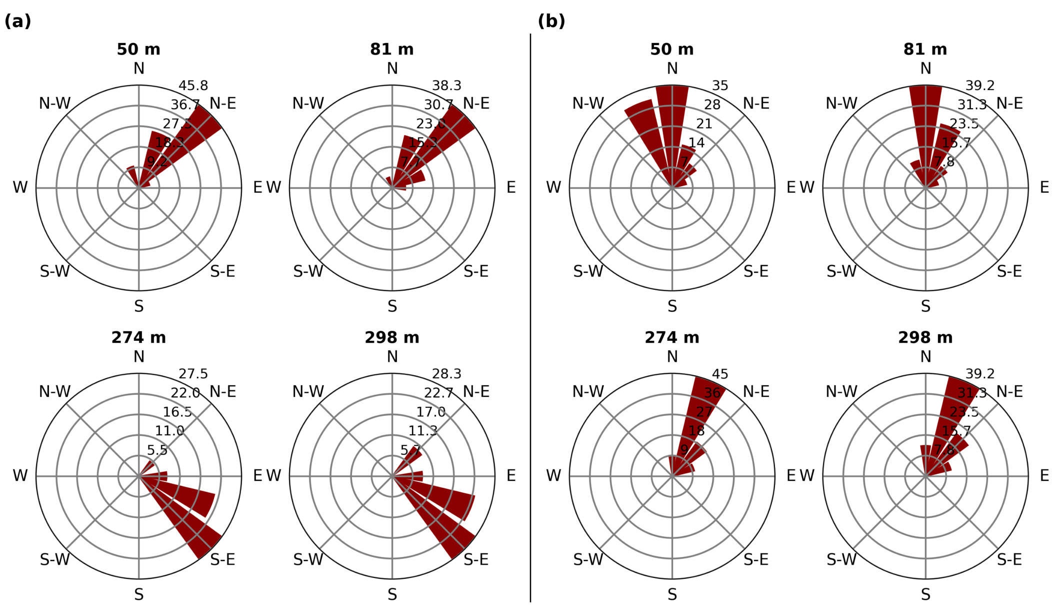

Figure 8. Wind direction at four distinct heights for a) 18 August 2022 and b) 25 August 2022.

surface-based nocturnal layer that remained partly decoupled from the air above, similar to the layered nocturnal structure described by Mahrt and Acevedo (2023). In contrast, the night of 25 August 2022 showed larger cloud cover (Fig. 9d and

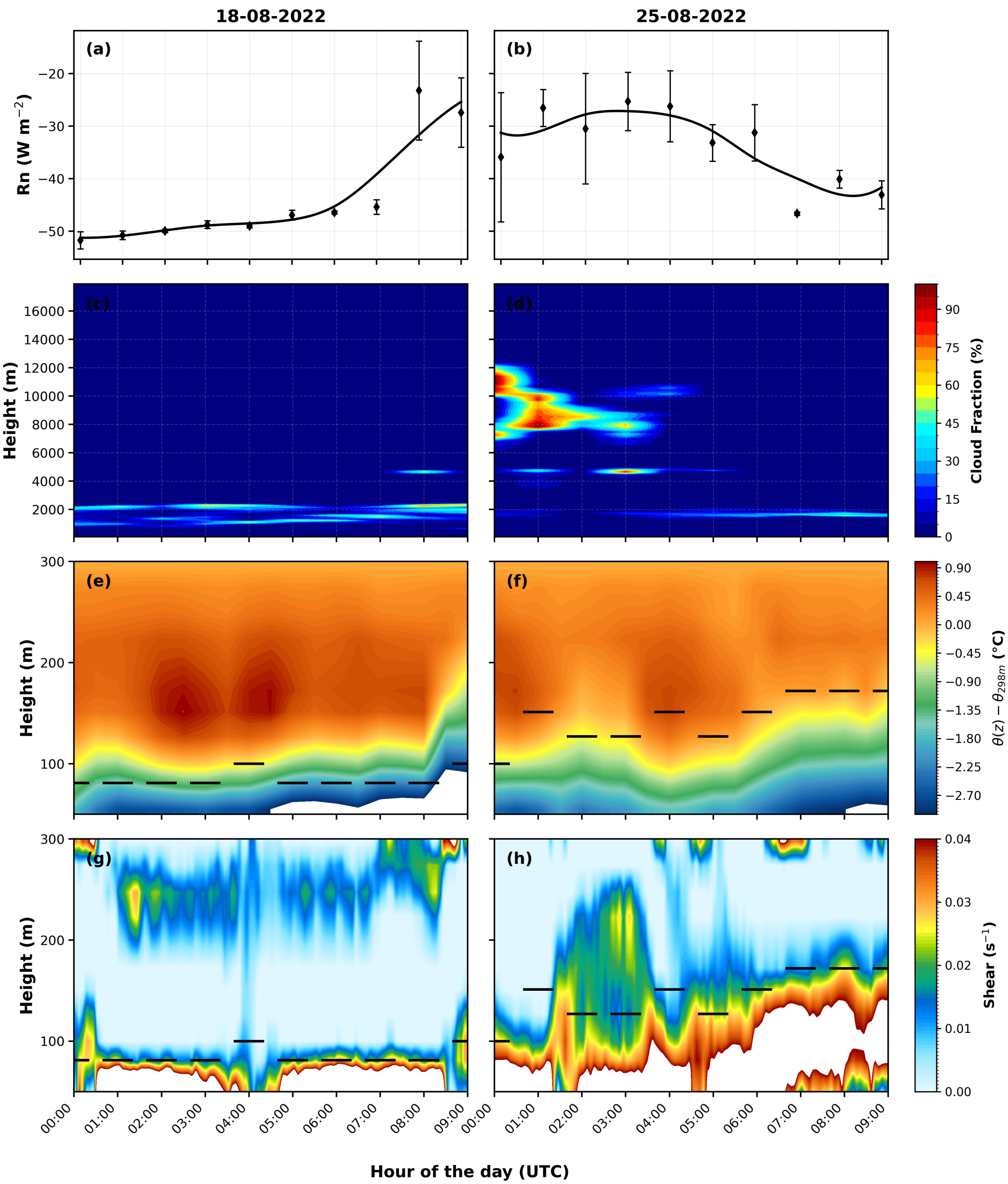

Figure 9. Nocturnal evolution of (a, b) hourly mean net radiation (R_n) at 81 m (± standard deviation), (c, d) cloud fraction (%), (e, f) vertical potential temperature (θ) difference from the value observed at 298 m, and (g, h) vertical wind shear (dU/dz) during the case-study nights of 18 August 2022 (left panels) and 25 August 2022 (right panels). Black horizontal segments indicate the estimated nocturnal boundary layer height at each hour.

Fig.S3), weaker radiative cooling during the early part of the night (Fig. 9b), and weaker thermal stratification (Fig. 9f). Wind shear extended to higher levels (Fig. 9h), reaching approximately 150–170 m, close to the observed h_n. This suggests that, under weaker stratification, mechanically generated turbulence was more effectively coupled over a deeper layer, contributing to the larger and more variable h_n observed during this night.

Figure 10 shows the CO and CH_4 concentrations for the two case studies. During the night of 18 August, the propagation of an air plume rich in CO and CH_4 that reached the tower was observed. However, this air mass was only detected by the inlets located at the highest heights (321 and 273 m), producing strong vertical differences in the tower CO and CH_4 profiles. The observation of elevated CO and CH_4 concentrations at higher altitudes, together with the different flow direction above the h_n (Figure 6 and 8), suggests that these air masses originated from more distant sources. Air arriving from the SE–S sector (above the NBL, Figure 6) likely transported high concentrations of CO and CH_4, possibly associated with regional biomass burning plumes (Andreae et al., 2015; Van Asperen et al., 2024) (Figure S4). In addition, it is believed that the plume did not penetrate down to canopy level (50 and 81 m) because the shallow h_n that night acted as a barrier (Figure 6). Meanwhile, air masses originating from the N–NE (below the NBL, Figure 6 and 8) exhibited lower CO and CH_4 concentration. We hypothesize that the height of 150 m is in the transition between the two layers, which explains why the CO and CH_4 concentrations coincide partly with those observed at 42 and 81 m. It is also noted that around 07:00 UTC the CO and CH_4 concentrations at the higher heights begin to decrease, reaching values similar to those observed at the lower heights at 09:00 UTC, which could indicate that the tower is leaving the concentration plume, caused by a change in wind direction at higher heights which shifted from SE–S to N–NE. To clarify, the layers remain decoupled, but the flow in both layers comes from the same direction and is no longer influenced by air masses with elevated CO and CH_4 concentration (Figure S4a).

On the night of 25 August, CO concentrations were higher than those observed on 18 August, indicating a multi-day pattern in which CO levels were generally elevated across the region (Figure S6), as more often observed in the region (Van Asperen et al., 2024). At 00:00 UTC on 25 August the highest CO and CH_4 concentrations were observed at the heights closest to the forest canopy, thereby different than at 18 August (Figure 10 b). Although plumes typically arrive first above the canopy, this apparent inversion can be explained by the slower response of air within the canopy to atmospheric changes. Elevated air from previous days (before 25 August; see Figure S5) may have penetrated the canopy, and while the passing plume quickly removed high concentrations from the upper layers, ventilation near the canopy occurred more slowly, resulting in higher concentrations at lower levels. Therefore, at 00:00 UTC, it appears that there is more CO and CH_4 at the lower levels, but this may simply reflect a delayed residual effect of a previous plume that has not yet been flushed out from the lower layers of the NBL. This is consistent with the difference in wind speed between heights, about $3\,m\,s^{-1}$ at 50 m and $5\,m\,s^{-1}$ at 150 m (Figure 7), suggesting slower air renewal at the lower levels.

One hour later (at 01:00 UTC) there is practically no difference between the CO and CH_4 concentrations at all measurement levels, remaining so until around 03:00 UTC. This behavior suggests that a new plume arrived at 01:00 UTC. It should be noted that at 03:00 UTC the CO and CH_4 concentrations at 321 m start to decrease, while at the lower levels there is a lag in this decrease. From 05:00 UTC the CO and CH_4 concentrations begin to decrease rapidly at the higher heights, while at the lower levels they decrease much slower. Overall, these two case studies highlight that the h_n is reflected in the vertical CO and CH_4

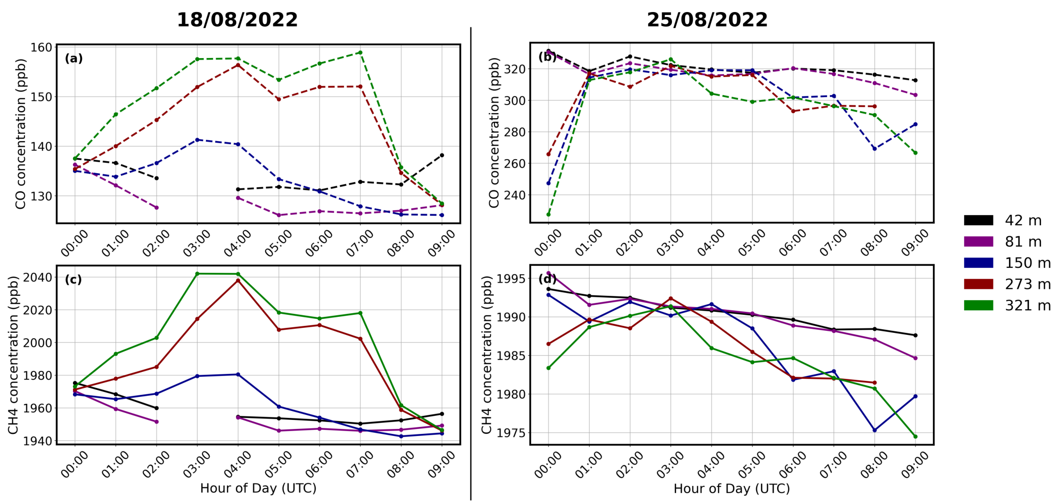

Figure 10. Vertical profiles of CO and CH_4 for the nights of 18 August 2022 and 25 August 2022. CO is shown in panels (a) and (b), and CH_4 in panels (c) and (d). Dashed lines indicate CO and solid lines indicate CH_4.

concentration profiles, thereby supporting our estimated h_n. When there is strong decoupling between the NBL and the layer above, air within the NBL can become trapped: the CO and CH_4 plume may be unable to enter the NBL, as on 18 August, or may be slow to ventilate out, as observed on 25 August.

4 Discussion

The results presented here demonstrate that the nocturnal boundary-layer height (h_n) above the central Amazon is strongly controlled by the interaction between nocturnal radiative cooling, atmospheric stability, cloud cover, and mechanically generated turbulence. Although previous Amazonian studies have primarily focused on the daytime evolution of the atmospheric boundary layer (Fisch et al., 2004; Carneiro and Fisch, 2020; Dias-Júnior et al., 2022), our results show that the nocturnal boundary layer also exhibits pronounced seasonal and interannual variability, with important implications for turbulence exchange and trace-gas transport above tropical forests.

One of the clearest patterns observed in this study is the systematic reduction of h_n during the Dry season and during the El Niño year (2023). These periods were characterized by stronger nocturnal net radiative loss (Figure 2a) and enhanced atmospheric stability, reflected by larger z/L values (Figure 2b) and a stronger thermal gradient (Fig. S6b, d). Under these conditions, turbulent exchange becomes increasingly suppressed, limiting the upward transport of sensible heat and favoring the formation of shallower nocturnal layers (Figures 4d and 5b). In contrast, wetter conditions, particularly during the Wet season of 2022, were associated with weaker radiative cooling (Figure 2a), reduced stability (Figure 2b), Weak thermal gradient (Fig S6a, c), and deeper nocturnal layers (Figures 4a and 5a). These findings reinforce the strong coupling between cloud cover, nocturnal cooling, and turbulence generation over the Amazon rainforest.

The hourly evolution of h_n also reveals the importance of the temporal evolution of thermal stratification during the night. In all analyzed periods, h_n was generally larger at the beginning of the night and progressively decreased toward the early morning hours (Figure 5). This behavior is particularly evident during the Wet season of 2022, when the thermal gradient remained relatively weak during the first hours of the night (Figures 9e,f and S6a), allowing mechanically generated turbulence to sustain a deeper nocturnal boundary layer. As the night progressed, radiative cooling intensified the thermal gradients, suppressing turbulence and leading to a gradual collapse of h_n.

The results also demonstrate that the interaction between thermal stratification and mechanically generated turbulence is fundamental for understanding the nocturnal boundary-layer structure above the Amazon forest (Figure 9). The case studies revealed that low-level jets (LLJs) (Figure 7) and enhanced vertical wind shear (Figure 9 g,h) may sustain turbulence above the canopy, but the influence of this turbulence on the lower nocturnal boundary layer depends on the degree of vertical coupling between atmospheric layers. This interpretation is consistent with the conceptual framework proposed by Mahrt and Acevedo (2023), in which nocturnal boundary layers may deviate from a vertically monotonic structure and instead exhibit layered configurations composed of shallow surface-based layers, transition layers, and elevated turbulent regions.

Our observations suggest that the forest canopy plays a key role in reinforcing this layered structure. Under strongly stable conditions, the canopy acts as a roughness and drag layer that attenuates momentum transfer toward the surface. Consequently, turbulence generated aloft by LLJs or strong wind shear may remain confined to elevated layers and may not efficiently penetrate downward through the canopy layer. This mechanism likely explains the shallow h_n observed on 18 August 2022, when strong thermal stratification and weak vertical coupling produced a highly decoupled nocturnal structure. In contrast, on 25 August 2022, weaker thermal stratification allowed mechanically generated turbulence to penetrate deeper into the lower nocturnal boundary layer, resulting in larger and more vertically connected h_n values.

Another important contribution of this study is the demonstration that variations in h_n are strongly reflected in the vertical distribution of trace gases such as CO and CH_4 (Figure 10). During nights characterized by shallow nocturnal layers, elevated concentrations observed at upper levels did not penetrate toward the canopy, suggesting that the nocturnal boundary layer acted as a barrier separating air masses above and below the canopy layer. Conversely, deeper nocturnal layers were associated with more vertically homogeneous concentration profiles, indicating enhanced turbulent mixing throughout the tower profile.

The interpretation of these concentration patterns must also consider the background atmospheric composition during previous days. As discussed by Botía et al. (2020), the ATTO site frequently experiences nighttime CH_4 accumulation associated with strong thermal stratification, suppressed turbulence, and horizontal transport from likely wetland source regions. In addition, CO concentrations are strongly influenced by regional biomass-burning plumes (Andreae et al., 2015; Van Asperen et al., 2024). For example, the elevated CO and CH_4 concentrations observed on 25 August 2022 likely reflected the residual influence of previous plume events (Figure S5) combined with slower ventilation near the canopy. Therefore, rather than associating multi-day concentration variability directly with h_n, our interpretation focuses on the short-term vertical concentration gradients and their relationship with nocturnal turbulent structure.

The additional case studies presented in the Supplement further reinforce this interpretation (Fig. S7). Strongly stable nights with shallow h_n (Fig. S8a) exhibited clear vertical separation between upper and lower layers (Fig. S7a,c), while less stable nights with deeper h_n (Fig S8b) showed much more homogeneous concentration patterns throughout the tower profile (Fig. S7b, d). The supplementary cases also show the importance of the initial/background concentrations from the previous days in shaping the nocturnal CO and CH_4 profiles (Fig. S9). As in the 18 and 25 August cases, the vertical gradients were influenced not only by the evolution of h_n, but also by the concentration structure already present before the night. These consistent relationships between h_n and the observed concentration gradients provide independent observational support for the turbulence-based estimates of nocturnal boundary-layer height presented here.

Compared to previous Amazonian studies, the turbulence-based methodology adopted in this work provides an important advantage because it estimates h_n directly from the vertical decay of turbulent sensible heat fluxes. Most previous studies relied on indirect methods based on thermodynamic profiles, Richardson number, or remote sensing approaches (Santos et al., 2007; Dias-Júnior et al., 2022; Carneiro et al., 2025). More recently, Mendonça et al. (2025) used the same turbulence-based methodology and reported h_n values ranging between approximately 81 and 223 m, demonstrating the importance of surface roughness and topography for nocturnal boundary-layer structure. However, their study did not focus on the hourly evolution of h_n or on its relationship with trace-gas concentration profiles. In addition, Huitema et al. (2026), using CloudRoots-Amazon22 observations (Vila-Guerau de Arellano et al., 2024), showed that multiple criteria based on potential temperature, CO_2, wind speed, Richardson number, and turbulent kinetic energy reproduce similar nocturnal boundary-layer dynamics, with estimated values between 114 and 241 m. The agreement between these independent approaches and the results presented here supports the robustness of the observed dynamic evolution of h_n at the ATTO site.

Finally, the results highlight the importance of continuous high-frequency vertical observations for understanding nocturnal processes above tropical forests. Stable nocturnal boundary layers strongly influence the transport of heat, moisture, aerosols, and greenhouse gases, and therefore directly affect weather prediction, atmospheric chemistry, and carbon-cycle studies over the Amazon Basin. Improving the representation of nocturnal turbulence and vertical coupling in atmospheric models is likely essential for reducing uncertainties in simulations of biosphere–atmosphere interactions in tropical forest regions.

5 Conclusions

This study presented the hourly variability of h_n heights during the Wet and Dry periods, based on turbulent data measured at the ATTO site (central Amazon) in a La Niña (2022) and an El Niño (2023) year. The results showed that the seasonal and interannual variability of h_n is mainly driven by the balance between nocturnal radiative cooling, atmospheric stability, cloud cover, and mechanically generated turbulence. Stronger radiative cooling and enhanced thermal stratification, especially during the Dry season and the El Niño year, favored shallower and more decoupled nocturnal layers, while weaker stability allowed turbulence generated by wind shear and low-level jets to sustain deeper and more vertically connected layers. Higher mean values were found in the Wet season under La Niña ($\sim 270 \pm 40$ m), while the lowest values occurred in the Dry season associated with El Niño ($\sim 100 \pm 27$ m). During the El Niño year, h_n varied from approximately 223 m at the beginning of the night to about 100 m at the end of the night. In contrast, in 2022, h_n ranged from roughly 274 m at the start of the night to 151 m at the end. Seasonal variability was also more evident at the beginning of the night in 2022 compared to 2023. Based on two case studies with contrasting conditions, the visibility of h_n on nighttime CO and CH_4 concentration profiles was explored: the first case study (18 August 2022) demonstrated a weak turbulence and a low h_n, and the second case study (25 August 2022) a stronger turbulence and a h_n progressively growing throughout the night. The case studies further revealed that a low h_n can cause a clear decoupling in air masses, resulting in contrasting concentration patterns along the tower, leading to strong vertical gradients (50 ppb for CH_4 and 10 ppb for CO). Conversely, with a higher h_n, concentration patterns along the tower remain more homogeneous, resulting in smaller gradients than in the first case. These results suggest that gas concentration profiles may be used as independent verification of the estimated boundary-layer heights.

Author contributions. Conceptualization: CMAS, ACSM, CQDJ, and HVA. Data curation: CQDJ, LGNM, HVA, RA and FAFD. Formal analysis: CMAS, HVA, and CQDJ. Funding acquisition: CQDJ and BTTP. Methodology: CMAS and ACSM. Project administration: CQDJ, BTTP, and CAQ. Software: CMAS. Supervision: CQDJ and SB. Validation: CMAS and HVA. Writing (original draft preparation): CMAS and CQDJ.Writing (review and editing): CMAS, SB, HVA, GF, FAFD, ACSM, RF, LRO, JRM, and DHH.

Competing interests. The authors declare that they have no competing interests.

Acknowledgements. This study is part of the Amazon Tall Tower Observatory (ATTO) project, which is supported by the German Federal Ministry of Education and Research (BMBF; contracts 01LB1001A and 01LK1602A), the Brazilian Ministry of Science, Technology and Innovation (MCTI/FINEP; contract 01.11.01248.00), and the Max Planck Society (MPG). Additional institutional support is provided by the Amazonas State Research Foundation (FAPEAM), the São Paulo State Research Foundation (FAPESP), the State University of Amazonas (UEA), the National Institute for Amazonian Research (INPA), the LBA Program, and the Secretariat of Sustainable Development (CEUC/RDS Uatumã). C. M. A. Souza acknowledges financial support from the Coordenação de Aperfeiçoamento de Pessoal de Nível Superior – Brasil (CAPES) through the Program in Climate and Environment (INPA/UEA; grant 88887.820693/2023-00). C. Q. Dias-Júnior acknowledges support from the Conselho Nacional de Desenvolvimento Científico e Tecnológico (CNPq; processes 440170/2022-8, 406884/2022-6, and 307530/2022-1). This study was also financed in part by CAPES – Finance Code 001 (grant 88881.933987/2024-01). We sincerely thank all partners involved in the long-term operation of the ATTO site for their continuous support. In particular, we acknowledge the essential logistical assistance provided by Roberta de Souza, Wallace Rabelo Costa, Nagib Alberto de Castro Souza, Amauri Rodrigues, Valmir Ferreira, and Antonio Huxley. We further thank the LBA micrometeorology group for their sustained commitment and technical efforts that made this work possible.

References

Andreae, M. O., Acevedo, O. C., Araùjo, A., Artaxo, P., Barbosa, C. G., Barbosa, H., Brito, J., Carbone, S., Chi, X., Cintra, B., et al.: The Amazon Tall Tower Observatory (ATTO): overview of pilot measurements on ecosystem ecology, meteorology, trace gases, and aerosols, Atmospheric Chemistry and Physics, 15, 10 723–10 776, 2015.

Barber, D. G. and Thomas, A.: The influence of cloud cover on the radiation budget, physical properties, and microwave scattering coefficient (σ) of first-year and multiyear sea ice, IEEE Transactions on Geoscience and Remote Sensing, 36, 38–50, 1998.

Barbosa, C. G., Taylor, P. E., Sá, M. O., Teixeira, P. R., Souza, R. A., Albrecht, R. I., Barbosa, H. M., Sebben, B., Manzi, A. O., Araújo, A. C., et al.: Identification and quantification of giant bioaerosol particles over the Amazon rainforest, npj Climate and Atmospheric Science, 5, 73, 2022.

Botía, S., Gerbig, C., Marshall, J., Lavric, J. V., Walter, D., Pöhlker, C., Holanda, B., Fisch, G., de Araújo, A. C., Sá, M. O., et al.: Understanding nighttime methane signals at the Amazon Tall Tower Observatory (ATTO), Atmospheric Chemistry and Physics, 20, 6583–6606, 2020.

Carneiro, R. G. and Fisch, G.: Observational analysis of the daily cycle of the planetary boundary layer in the central Amazon during a non-El Niño year and El Niño year (GoAmazon project 2014/5), Atmospheric Chemistry and Physics, 20, 5547–5558, 2020.

Carneiro, R. G., Ribeiro, M. M., Gatti, L. V., de Souza, C. M. A., Dias-Júnior, C. Q., Tejada, G., Domingues, L. G., Rykowska, Z., dos Santos, C. A., and Fisch, G.: Assessing the effectiveness of convective boundary layer height estimation using flight data and ERA5 profiles in the Amazon biome, Climate Dynamics, 63, 109, 2025.

Cava, D., Dias-Júnior, C. Q., Acevedo, O., Oliveira, P. E., Tsokankunku, A., Sörgel, M., Manzi, A. O., de Araújo, A. C., Brondani, D. V., Toro, I. M. C., et al.: Vertical propagation of submeso and coherent structure in a tall and dense Amazon Forest in different stability conditions PART I: Flow structure within and above the roughness sublayer, Agricultural and Forest Meteorology, 322, 108 983, 2022.

Chamecki, M., Freire, L. S., Dias, N. L., Chen, B., Dias-Junior, C. Q., Toledo Machado, L. A., Sörgel, M., Tsokankunku, A., and Araújo, A. C. d.: Effects of vegetation and topography on the boundary layer structure above the Amazon forest, Journal of the Atmospheric Sciences, 77, 2941–2957, 2020.

De Oliveira, G., Brunsell, N. A., Moraes, E. C., Bertani, G., Dos Santos, T. V., Shimabukuro, Y. E., and Aragão, L. E.: Use of MODIS sensor images combined with reanalysis products to retrieve net radiation in Amazonia, Sensors, 16, 956, 2016.

Dias, N. L., Toro, I. M. C., Dias-Júnior, C. Q., Mortarini, L., and Brondani, D.: The relaxed eddy accumulation method over the amazon forest: the importance of flux strength on individual and aggregated flux estimates, Boundary-Layer Meteorology, 189, 139–161, 2023.

Dias-Júnior, C. Q., Dias, N. L., dos Santos, R. M. N., Sörgel, M., Araújo, A., Tsokankunku, A., Ditas, F., de Santana, R. A., Von Randow, C., Sá, M., et al.: Is there a classical inertial sublayer over the amazon forest?, Geophysical Research Letters, 46, 5614–5622, 2019.

Dias-Júnior, C. Q., Carneiro, R. G., Fisch, G., D'Oliveira, F. A. F., Sörgel, M., Botía, S., Machado, L. A. T., Wolff, S., Santos, R. M. N. d., and Pöhlker, C.: Intercomparison of planetary boundary layer heights using remote sensing retrievals and ERA5 reanalysis over Central Amazonia, Remote Sensing, 14, 4561, 2022.

Dias-Junior, C. Q., Marques Filho, E. P., Araújo, A., Mendonça, A. C. S., Hall, D. H., Santana, R. A. S. d., D'Oliveira, F. A. F., Fisch, G., Acevedo, O., Dias, N. L., Oliveira, P. E., Souza, C. M. A., Figueiredo, R., Farias, C. d. S., Ramos de Oliveira, L., Ramos da Mata, J., de Lima Xavier, T., Teixeira, P. R., Tanaka Portela, B. T., Alves, E. G., Botía, S., van Asperen, H., Komiya, S., Andreae, M. O., Sörgel, M., Trumbore, S., Manzi, A., and Quesada, C. A.: Characterizing long-term meteorological and flux variability of an old-growth tropical forest in the Central Amazon: a decade of ATTO tower observations, Available at SSRN, https://doi.org/10.2139/ssrn.6468680, 2026.

Driedonks, A.: Models and observations of the growth of the atmospheric boundary layer, Boundary-Layer Meteorology, 23, 283–306, 1982.

Fisch, G., Tota, J., Machado, L., Silva Dias, M. A. F. d., Da F. Lyra, R., Nobre, C., Dolman, A., and Gash, J.: The convective boundary layer over pasture and forest in Amazonia, Theoretical and Applied Climatology, 78, 47–59, 2004.

Foken, T. and Mauder, M.: Micrometeorology, vol. 2, Springer, 2008.

Franco, M. A., Valiati, R., Holanda, B. A., Meller, B. B., Kremper, L. A., Rizzo, L. V., Carbone, S., Morais, F. G., Nascimento, J. P., Andreae, M. O., et al.: Vertically resolved aerosol variability at the Amazon Tall Tower Observatory under wet-season conditions, Atmospheric Chemistry and Physics, 24, 8751–8770, 2024.

Gao, W., Shaw, R., and Paw U, K.: Observation of organized structure in turbulent flow within and above a forest canopy, Boundary-Layer Meteorology, 47, 349–377, 1989.

Garratt, J.: Surface influence upon vertical profiles in the atmospheric near-surface layer, Quarterly Journal of the Royal Meteorological Society, 106, 803–819, 1980.

Gomes Alves, E., Aquino Santana, R., Quaresma Dias-Júnior, C., Botía, S., Taylor, T., Yáñez-Serrano, A. M., Kesselmeier, J., Bourtsoukidis, E., Williams, J., Lembo Silveira de Assis, P. I., et al.: Intra-and interannual changes in isoprene emission from central Amazonia, Atmospheric Chemistry and Physics, 23, 8149–8168, 2023.

Guo, J., Miao, Y., Zhang, Y., Liu, H., Li, Z., Zhang, W., He, J., Lou, M., Yan, Y., Bian, L., et al.: The climatology of planetary boundary layer height in China derived from radiosonde and reanalysis data, Atmospheric Chemistry and Physics, 16, 13 309–13 319, 2016.

Huitema, A. C., de Feiter, V. S., González-Armas, R., Hartogensis, O. K., van Asperen, H., Quaresma Dias-Júnior, C., and Vilà-Guerau de Arellano, J.: CO_2 and Heat exchange across the Nocturnal Canopy–Atmosphere interface in the Amazon rainforest, EGUsphere, 2026, 1–32, 2026.

Jimenez, J. C., Libonati, R., and Peres, L. F.: Droughts over Amazonia in 2005, 2010, and 2015: A cloud cover perspective, Frontiers in Earth Science, 6, 227, 2018.

Kaimal, J. C. and Finnigan, J. J.: Atmospheric boundary layer flows: their structure and measurement, Oxford university press, 1994.

Keirsbulck, L., Labraga, L., Mazouz, A., and Tournier, C.: Surface roughness effects on turbulent boundary layer structures, J. Fluids Eng., 124, 127–135, 2002.

Krishnamurthy, R., Newsom, R. K., Berg, L. K., Xiao, H., Ma, P.-L., and Turner, D. D.: On the estimation of boundary layer heights: a machine learning approach, Atmospheric Measurement Techniques Discussions, 2020, 1–34, 2020.

Kulmala, M., Kokkonen, T., Ezhova, E., Baklanov, A., Mahura, A., Mammarella, I., Bäck, J., Lappalainen, H. K., Tyuryakov, S., Kerminen, V.-M., et al.: Aerosols, clusters, greenhouse gases, trace gases and boundary-layer dynamics: on feedbacks and interactions, Boundary-Layer Meteorology, 186, 475–503, 2023.

Lenschow, D. H., Li, X. S., Zhu, C. J., and Stankov, B. B.: The stably stratified boundary layer over the Great Plains: I. Mean and turbulence structure, Boundary-layer meteorology, 42, 95–121, 1988.

Levi, Y., Dayan, U., Levy, I., Broday, D. M., et al.: On the association between characteristics of the atmospheric boundary layer and air pollution concentrations, Atmospheric Research, 231, 104 675, 2020.

Mahrt, L. and Acevedo, O.: Types of vertical structure of the nocturnal boundary layer, Boundary-Layer Meteorology, 187, 141–161, 2023.

Marengo, J. A., Liebmann, B., Kousky, V. E., Filizola, N. P., and Wainer, I. C.: Onset and end of the rainy season in the Brazilian Amazon Basin, Journal of Climate, 14, 833–852, 2001.

Marengo, J. A., Souza Jr, C. M., Thonicke, K., Burton, C., Halladay, K., Betts, R. A., Alves, L. M., and Soares, W. R.: Changes in climate and land use over the Amazon region: current and future variability and trends, Frontiers in Earth Science, 6, 228, 2018.

Mendonça, A. C., Dias-Junior, C. Q., Acevedo, O. C., Marra, D. M., Cely-Toro, I. M., Fisch, G., Brondani, D. V., Manzi, A. O., Portela, B. T., Quesada, C. A., et al.: Estimation of the nocturnal boundary layer height over the Central Amazon forest using turbulence measurements, Agricultural and Forest Meteorology, 367, 110 469, 2025.

Mendonça, A. C., Dias-Junior, C. Q., de Oliveira, M. I., Maroneze, R., Martins, L. G. N., Marra, D. M., D'Oliveira, F. A. F., Costa, F. D., Fisch, G., Hall, D. H., et al.: Is Low-Level Jet height a good approximation for the top of the nocturnal boundary-layer?, Agricultural and Forest Meteorology, 380, 111 065, https://doi.org/10.1016/j.agrformet.2026.111065, 2026.

Miao, Y., Hu, X.-M., Liu, S., Qian, T., Xue, M., Zheng, Y., and Wang, S.: Seasonal variation of local atmospheric circulations and boundary layer structure in the Beijing-Tianjin-Hebei region and implications for air quality, Journal of Advances in Modeling Earth Systems, 7, 1602–1626, 2015.

Molero, F., Barragán, R., and Artíñano, B.: Estimation of the atmospheric boundary layer height by means of machine learning techniques using ground-level meteorological data, Atmospheric Research, 279, 106 401, 2022.

Oliveira, P. E., Acevedo, O. C., Sörgel, M., Tsokankunku, A., Wolff, S., Araújo, A. C., Souza, R. A., Sá, M. O., Manzi, A. O., and Andreae, M. O.: Nighttime wind and scalar variability within and above an Amazonian canopy, Atmospheric Chemistry and Physics, 18, 3083–3099, 2018.

Restrepo-Coupe, N., O'Donnell Christoffersen, B., Longo, M., Alves, L. F., Campos, K. S., da Araujo, A. C., de Oliveira Jr, R. C., Prohaska, N., da Silva, R., Tapajos, R., et al.: Asymmetric response of Amazon forest water and energy fluxes to wet and dry hydrological extremes reveals onset of a local drought-induced tipping point, Global Change Biology, 29, 6077–6092, 2023.

Santana, R. A., Dias-Júnior, C. Q., da Silva, J. T., Fuentes, J. D., do Vale, R. S., Alves, E. G., dos Santos, R. M. N., and Manzi, A. O.: Air turbulence characteristics at multiple sites in and above the Amazon rainforest canopy, Agricultural and Forest Meteorology, 260, 41–54, 2018.

Santos, R. M. N., Fisch, G., and Dolman, A.: Modelagem da camada limite noturna (CLN) durante a época úmida na Amazônia, sob diferentes condições de desenvolvimento, Revista brasileira de meteorologia, 22, 387–407, 2007.

Shaw, R. H. and Schumann, U.: Large-eddy simulation of turbulent flow above and within a forest, Boundary-Layer Meteorology, 61, 47–64, 1992.

Souza, C. M. A., Dias-Júnior, C. Q., D'Oliveira, F. A. F., Martins, H. S., Carneiro, R. G., Portela, B. T. T., and Fisch, G.: Long-term measurements of the atmospheric boundary layer height in central Amazonia using remote sensing instruments, Remote Sensing, 15, 3261, 2023.

Starkenburg, D., Metzger, S., Fochesatto, G. J., Alfieri, J. G., Gens, R., Prakash, A., and Cristóbal, J.: Assessment of despiking methods for turbulence data in micrometeorology, Journal of Atmospheric and Oceanic Technology, 33, 2001–2013, 2016.

Su, T., Li, Z., and Kahn, R.: Relationships between the planetary boundary layer height and surface pollutants derived from lidar observations over China: regional pattern and influencing factors, Atmospheric Chemistry and Physics, 18, 15 921–15 935, 2018.

Sun, J., Burns, S. P., Lenschow, D. H., Banta, R., Newsom, R., Coulter, R., Frasier, S., Ince, T., Nappo, C., Cuxart, J., et al.: Intermittent turbulence associated with a density current passage in the stable boundary layer, Boundary-Layer Meteorology, 105, 199–219, 2002.

van Asperen, H., Komiya, S., Jones, S., Botia, S., Lavric, J., Warneke, T., Griffith, D., and Trumbore, S.: Unique Tall Tower Greenhouse Gas Measurements in the Amazon Rainforest: observed patterns and daily cycles, in: EGU General Assembly Conference Abstracts, pp. EGU–10 522, 2023.

Van Asperen, H., Warneke, T., Carioca de Araújo, A., Forsberg, B., José Filgueiras Ferreira, S., Röckmann, T., Van Der Veen, C., Bulthuis, S., Ramos de Oliveira, L., de Lima Xavier, T., et al.: The emission of CO from tropical rainforest soils, Biogeosciences, 21, 3183–3199, 2024.

Vila-Guerau de Arellano, J., Hartogensis, O., De Boer, H., Moonen, R., González-Armas, R., Janssens, M., Adnew, G., Bonell-Fontás, D., Botía, S., Jones, S., et al.: CloudRoots-Amazon22: Integrating clouds with photosynthesis by crossing scales, Bulletin of the American Meteorological Society, 105, E1275–E1302, 2024.

Von Randow, C., Manzi, A. O., Kruijt, B., De Oliveira, P., Zanchi, F. B., Silva, R. d., Hodnett, M. G., Gash, J. H., Elbers, J. A., Waterloo, M., et al.: Comparative measurements and seasonal variations in energy and carbon exchange over forest and pasture in South West Amazonia, Theoretical and Applied Climatology, 78, 5–26, 2004.

Wang, L., Liu, J., Gao, Z., Li, Y., Huang, M., Fan, S., Zhang, X., Yang, Y., Miao, S., Zou, H., et al.: Vertical observations of the atmospheric boundary layer structure over Beijing urban area during air pollution episodes, Atmospheric Chemistry and Physics, 19, 6949–6967, 2019.

Webb, E. K., Pearman, G. I., and Leuning, R.: Correction of flux measurements for density effects due to heat and water vapour transfer, Quarterly Journal of the Royal Meteorological Society, 106, 85–100, 1980.

Wilczak, J. M., Oncley, S. P., and Stage, S. A.: Sonic anemometer tilt correction algorithms, Boundary-layer meteorology, 99, 127–150, 2001.

Zahn, E., Chor, T., and Dias, N.: A simple methodology for quality control of micrometeorological datasets, Am J Environ Eng, 6, 135–142, 2016.